Cerebral Cortex, September 2020;30: 4858–4870

doi: 10.1093/cercor/bhaa078
Advance Access Publication Date: 5 May 2020
Original Article

ORIGINAL ARTICLE

Mutation Carriers with Reduced C-Afferent Density Reveal Cortical Dynamics of Pain–Action Relationship during Acute Pain

I. Perini[1], M. Ceko[2], L. Cerliani[3,4], H. van Ettinger-Veenstra[1], J. Minde[5] and I. Morrison[1]

[1]Department of Clinical and Experimental Medicine, Center for Social and Affective Neuroscience, Linköping University, Linköping 581 83, Sweden, [2]Institute of Cognitive Science, University of Colorado, Boulder, CO 80309, USA, [3]Brain Connectivity and Behaviour Group, Frontlab, Institut du Cerveau et de la Moelle épinière (ICM), UMRS 975, 75013 Paris, France, [4]Department of Psychiatry, Academic Medical Centre, Amsterdam Brain and Cognition, University of Amsterdam, 1000 GG Amsterdam, Netherlands and [5]Department of Surgery, Unit of Orthopedics, Perioperative Sciences, Umeå University Hospital, Umeå S-901 85, Sweden

Address correspondence to I. Morrison. Email: india.morrison@liu.se

Abstract

The evidence that action shapes perception has become widely accepted, for example, in the domain of vision. However, the manner in which action-relevant factors might influence the neural dynamics of acute pain processing has remained underexplored, particularly the functional roles of anterior insula (AI) and midanterior cingulate cortex (mid-ACC), which are frequently implicated in acute pain. To address this, we examined a unique group of heterozygous carriers of the rare R221W mutation on the nerve growth factor (NGF) gene. R221W carriers show a congenitally reduced density of C-nociceptor afferent nerves in the periphery, but can nonetheless distinguish between painful and nonpainful stimulations. Despite this, carriers display a tendency to underreact to acute pain behaviorally, thus exposing a potential functional gap in the pain–action relationship and allowing closer investigation of how the brain integrates pain and action information. Heterozygous R221W carriers and matched controls performed a functional magnetic resonance imaging (fMRI) task designed to dissociate stimulus type (painful or innocuous) from current behavioral relevance (relevant or irrelevant), by instructing participants to either press or refrain from pressing a button during thermal stimulation. Carriers' subjective pain thresholds did not differ from controls', but the carrier group showed decreased task accuracy. Hemodynamic activation in AI covaried with task performance, revealing a functional role in pain–action integration with increased responses for task-relevant painful stimulation ("signal," requiring button-press execution) over task-irrelevant stimulation ("noise," requiring button-press suppression). As predicted, mid-ACC activation was associated with action execution regardless of pain. Functional connectivity between AI and mid-ACC increased as a function of reported urge to withdraw from the stimulus, suggesting a joint role for these regions in motivated action during pain. The carrier group showed greater activation of primary sensorimotor cortices—but not the AI and mid-ACC regions—during pain and action, suggesting compensatory processing. These findings indicate a critical role for the AI–mid-ACC axis in supporting a flexible, adaptive action selection during pain, alongside the accompanying subjective experience of an urge to escape the pain.

Key words: action, anterior cingulate cortex, anterior insula, pain, R221W mutation

Introduction

Acute pain carries a potent ability to influence action, not least by perturbing ongoing voluntary behavior. But the functional neuroanatomy of the relationship between sensory processing and action selection during pain remains unclear. In a traditional view of pain, exemplified by Descartes' mechanistic model (Descartes 1632, translated in Hall 1972), the brain identifies a stimulus as "pain" on the basis of afferent nerve signaling, with a consequent behavioral response largely determined by the noxious nature and experiential content of the sensory signal (for discussion and critique of this premise in modern neuroscience, see Sullivan 2008).

Yet a growing body of human neuroimaging studies belies the simplicity of that model, showing instead that cortical representation of pain is not straightforwardly driven by sensory input (Seminowicz et al. 2004; Atlas et al. 2010; Perini et al. 2013; Wiech et al. 2014; Taylor et al. 2017; Woo et al. 2017; Knudsen et al. 2018; Lopez-Sola et al. 2019). Further, the general perspective that action goals influence sensory perception has become widely accepted in recent decades, for example, in the interplay between vision and action (e.g., Prinz, 1997; Nöe, 2004; Grush, 2004). However, this idea has not been extensively explored in the case of acute pain, despite indications that pain processing is interlinked with behavior and action (Shackman et al. 2011; Morrison et al. 2013; Wiech and Tracey 2013). This study therefore investigates the pain–action relationship in the human cortex and the extent to which pain processing may be flexibly shaped by current demands on behavior.

To disentangle any cortical-level integration of pain signaling and action, we manipulated whether a stimulus was relevant to current action goals, by using a paradigm in which painful thermal stimulation was relevant to the button-press task in half the trials (pain as "signal") and irrelevant in the other half (pain as "noise") (Perini et al. 2013). If cortical pain processing were driven primarily by stimulus information, such task variables should not modulate behavioral or neural responses. On the other hand, if the brain's response to pain reflects integrative processing of both stimulus- *and* task-relevant factors, changing the task relevance of acute pain should affect these responses. In a previous experiment, this paradigm revealed specific neural activations that hinged on action-related processing regardless of pain, for example, in midanterior cingulate cortex (mid-ACC or MCC). This suggested that certain regional brain activity during pain can be accounted for by an action variable: whether the situation demands the execution or suppression of a given behavior.

However, manipulating an action variable does not wholly address how the stimulus signal from the periphery may be integrated with action demands in the cortex, especially in particular pain-related regions that show preferential responses to pain regardless of overt behavioral outcome, such as anterior insula (AI) (Perini et al. 2013). Previous research in healthy populations has implemented higher-level task manipulations during at- or under-threshold painful stimulation (Sinke et al. 2016; Zaman et al. 2018), demonstrating interactions between task-driven expectations and cortical pain processing. A more direct probe of the relative contribution of a stimulus variable to cortical pain–action integration would require manipulation of the stimulus-evoked signal, for example, through attenuation or ambiguation. Yet a more "bottom-up" manipulation of above-threshold painful stimuli—without impairing an ability to identify the stimulus as painful—would be difficult in healthy individuals, for whom above-threshold painful stimulation is robustly salient and comes with an inherently behaviorally relevant motivational component. We therefore turned to a population in which nociceptive signaling from the periphery was likely to be attenuated or ambiguated, potentially affecting motivational and behavioral reactions to pain, but without severe effects on the ability to identify a stimulus as subjectively painful.

Heterozygous carriers of the R221W mutation (also called R100W (Sung et al. 2018; Testa et al. 2019) on the nerve growth factor (NGF) gene exhibit a congenitally reduced density of nociceptive C-afferent nerves in the periphery (Minde et al. 2004; Larsson et al. 2009; Perini et al. 2016). The mutation can therefore be regarded as reduction of function in the adult phenotype, with fewer typically functioning C-nociceptor afferents in the skin. Variability in R221W carrier peripheral C nerve fiber density (C-NFD) has also correlated with variability on clinical and subjective measures of pain report (Perini et al. 2016). Yet critically, heterozygous R221W carriers have shown a normal ability to distinguish descriptions of painful from nonpainful situations, but nonetheless report significantly lower estimates of *how* painful they would find a given noxious stimulus (Perini et al. 2016).

This crucial population-level dissociation in R221W heterozygotes, with altered subjective pain evaluation alongside typical-range sensory discrimination, informed two parallel hypotheses for the present study. First, reduced C-afferent density would allow investigation of how the brain integrates the nociceptive signal in the service of producing a situation-appropriate behavioral response, potentially exposing underlying cortical dynamics of a pain–action relationship. Second, it may address whether the tendency for pain underestimation previously observed in R221W carriers can be explained by a simple sensory deficit or by a more complex decrement in the cortical integration of nociceptive information with motivated behavior. These two hypotheses could be jointly addressed in this study because the upper part of heterozygotes' C-NFD variability overlaps with that of the healthy phenotype (Perini et al. 2016). This implies that variance or skew in the carrier group's phenotypic range could offer a valuable glimpse into typical functional neuroanatomy, providing statistical traction for investigating features of the underlying functional processing, as well as any compensatory processing.

To explore these questions, we compared a group of heterozygous R221W carriers with age-, sex-, and education-matched controls, using an experimental paradigm dissociating the painfulness of a stimulus from its behavioral relevance to a current task (Perini et al. 2013). We expected that, in R221W carriers, both behavior- and cortical-level responses in pain-related regions including mid-ACC (implicated in the action component of pain), and AI (implicated in pain but also in stimulus salience and task-set maintenance (e.g., Dosenbach et al. 2008; Uddin 2015), would be altered or attenuated.

Materials and Methods

Participants

Twelve heterozygous R221W carriers (seven females, mean age 36.2; ± standard deviation [SD] 15.4) and twelve gender-, age-, and education-matched controls gave informed consent in accordance with the Declaration of Helsinki. This mutation is rare, with ~50 adult carriers currently identified by genetic

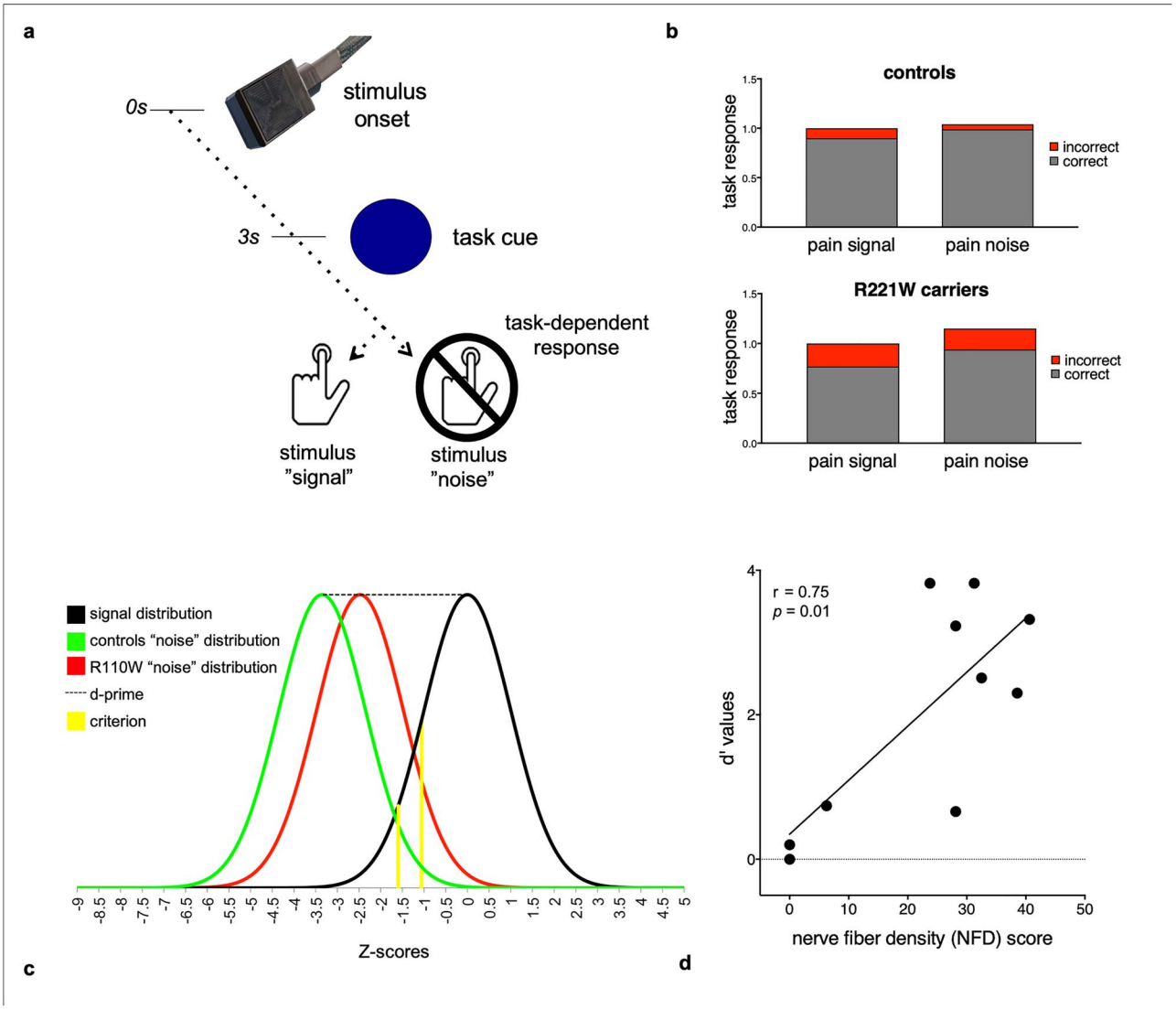

Figure 1. Experimental design and task performance. (*a*) In each trial, a painful or nonpainful thermal stimulus was applied to the dorsum of the hand for 4 s. During stimulation a task cue (dot) appeared, and participants responded by speeded button press, depending on instructions indicating whether the stimulus was to be considered "signal" or "noise." In signal trials a button press was required by the task, while in noise trials task instructions required participants to refrain from pressing the button. (*b*) Heterozygous R221W carriers made more total button-press errors than controls in distinguishing signal from noise during painful stimulation ($P < 0.001$). (*c*) Signal and noise distributions for heterozygous R221W carriers and controls exhibited wider separation between signal and noise (task sensitivity, d′) for controls than carriers. (*d*) d′ covaried with R221W carriers' C-afferent nerve fiber density (C-NFD), indicating a relationship between behavioral and C-afferent phenotype. To illustrate the full range of task performance variance in the R221W mutation phenotype, additional data from a separate dataset of three homozygous R221W carriers were included.

screening and mainly confined to a geographic area in the far north of Sweden. Carriers were identified by pedigree, and the presence of the mutation (an arginine-to-tryptophan substitution) on one allele of the beta subunit of the NFG gene was confirmed by DNA sequencing. All data were collected at the Umeå Center for Functional Brain Imaging, Umeå University Hospital (Umeå, Sweden). Carriers of the R221W mutation were compensated at 200 SEK/h, along with travel expenses and any lost work income. Local control volunteers did not need to travel and were compensated at 200 SEK/h. Previously collected data from three homozygous R221W carriers (one female, mean age 35.3 [±SD 22.5]) were included in the correlational analysis presented in Figure 1*d*.

MRI Acquisition

Data were collected using a 3-T General Electric (GE) Discovery MR 750 scanner with a 32-channel head coil. A gradient-echo echo-planar imaging (EPI) sequence was used to acquire the whole-brain functional images (repetition time [TR] = 3000 ms; echo time [TE] = 35 ms; flip angle = 90°; field of view [FOV] = 128 × 128; 46 axial slices; in-plane resolution = 1.9 × 1.9 mm; slice thickness = 2.9 mm). A high-resolution T_1-weighted scan was acquired to aid registration of the EPI images to standard space and to be used for cortical thickness analysis: TR = 8.2 ms; TE = 1.5 ms; flip angle = 12°; field of view = 256 × 256; in-plane resolution = 0.4 × 0.4 mm; slice thickness = 1 mm; and number of axial slices = 64.

Experimental Design

The task and functional magnetic resonance imaging (fMRI) paradigm were adapted from Perini et al. (2013) (Fig. 1*a*). The paradigm was a 2 × 2 factorial design, with the factors pain (noxious, innocuous) and motor response (press, no press). In each of the 48 trials, noxious or innocuous heat stimuli were delivered with a 30 x 30-mm thermal stimulator probe (PATHWAY Model Advanced Thermal Stimulator [ATS], Medoc Ltd, Ramat Yishai, Israel) for a 4-s plateau of target temperature on the dorsal part of the left hand. Moderately painful heat and nonpainful warm temperatures were used.

The stimuli were delivered in a counterbalanced order in two separate runs. In half the trials, participants were instructed to press a button when a cue appeared only if the stimulus was painful ("pain signal") and in the other half only if it was nonpainful ("pain noise"). The task cue (dot) appeared 1 s before stimulus offset. Because the design aimed to capture general motor facilitation, stimulation was delivered to the nonresponse (left) hand to reduce potential confounds between stimulus- and response-related activations and to limit any effects of thermode application on button-press fluency. Responses were made with the right hand using a response pad system (4-Button Diamond Fiber Optic Response Pad, Current Designs Inc., Philadelphia, United States). The painful temperature threshold was determined for each participant before the fMRI session by identifying the temperature rated as 8 on a numeric rating scale (8 on a numeric rating scale [NRS], with anchors 0 = no pain; 10 = intense pain). Similarly, the nonpainful temperature was determined for each participant by identifying the reported threshold temperature between warmth and 32 °C cold.

This forced-choice task presented four possible responses, two for each stimulus. Two of the four possibilities reflected correct responses (i.e., "hits" and "correct rejections"), whereas the other two reflected errors (i.e., "misses" and "false alarms") (Green and Swets 1966; Wickens 2001). We examined the frequency of correct (hits) and incorrect (misses, false alarms) responses, regardless of stimulus type, between groups. We further examined the two groups' sensitivity to task requirements (d′), on the basis of correct button presses (hits) and incorrect button presses (false alarms). The higher the d′ score, the greater the distance between "signal" and "noise" distributions, and hence the clearer the separation in responses. d′ prime scores were calculated by subtracting the Z-transformed false alarms from the Z-transformed hits, divided by the group's SD, for each participant. Criterion scores, reflecting the threshold of differentiation between signal and noise distributions, were also calculated for each individual and compared between groups. Criterion is an orthogonal score calculated using the same hit and false alarm values, reflecting whether participants were more likely to respond to signal or to noise. The further the criterion shift into the signal or noise distribution, the greater the bias for responding to signal or noise.

Following the fMRI session, "urge to move" ratings were obtained (see also Perini et al. 2013). The trial structure was identical to that of the fMRI paradigm, with a total of six painful (hot) and six nonpainful (warm) thermal stimulations on the dorsal part of the left hand. Participants held a mouse in their right hand and were instructed to continuously rate their subjective urge to move their hand away from the thermode, by dragging the mouse on a visual analog scale (VAS) displayed on a computer screen, with anchor points "no urge" (1) and "high urge" (10). To investigate the pattern of continuous ratings over time, each rating was fitted to a linear regression, and the slope value was calculated. The mean slope values were then compared between R221W carriers and control groups (Fig. 2*d*).

Statistical Analysis of Functional MRI Data

fMRI analysis was performed using the FMRIB Software Library (FMRIB, Oxford, United Kingdom; www.fmrib.ox.ac.uk/fsl). fMRI data analysis was carried out using FEAT (FMRI Expert Analysis Tool) version 6.00. The following prestatistics processing was applied: motion correction using Motion Correction FMRIB Linear Registration Tool (MCFLIRT) (Jenkinson et al. 2002), non-brain removal using Brain Extraction Tool (BET) (Smith 2002), spatial smoothing using a Gaussian kernel of full width at half maximum (FWHM) 8 mm, grand-mean intensity normalization of the entire 4D dataset by a single multiplicative factor, and high-pass temporal filtering (Gaussian-weighted least-squares straight line fitting, with sigma = 50.0 s). Predictors for the four events (cue, nonpainful stimulation, painful stimulation, and button-press response) were created for each subject and each run and added to the first-level time-series statistical analysis. Time-series statistical analysis was carried out using FMRIB's Improved Linear Model (FILM) with local autocorrelation correction. Higher-level analysis applied a fixed-effects model, with the assumption that individual-specific effects would likely be correlated with the independent variables in the carrier group, based on previous observations on this unique population in which C-NFD correlated with various outcome measures (Perini et al. 2016), and also because the composition of the control group (age, gender, education level) was matched to the carrier group on an individual level. The previous normative study was analyzed with random effects, so we are confident that the effects in the control group, which replicated the previous effects, were not driven by individual differences. This higher-level fixed-effects analysis was performed using FEAT version 6.00 by forcing the random effects variance to zero in FLAME (FMRIB's Local Analysis of Mixed Effects) (Beckmann et al. 2003; Woolrich et al. 2004; Woolrich 2008). Z statistic images were thresholded using clusters determined by $Z > 3$ and a (corrected) cluster significance threshold of $P = 0.01$, using the Gaussian random field (GRF) theory (Worsley 2011).

An additional conjunction analysis, based on the study by Perini et al. (2013), was performed to verify the reproducibility of the previous findings in healthy controls (formerly modeled with BrainVoyager software), as well as complementing analysis of the differences between R221W carriers and controls. For each participant, four predictors that modeled each of the following four conditions across runs were created: painful heat press, painful heat no-press, nonpainful heat press, and nonpainful heat no-press (Perini et al. 2013).

Finally, to investigate which features of cortical organization might differentiate R221W carriers in the healthy range from those with lower performance, we performed a within-group analysis testing in any continuous covariate interaction between task sensitivity scores (d′) and blood-oxygen-level–dependent (BOLD) signal change during pain stimulation. The analysis was restricted to the bilateral insula, independently defined using the Montreal Neurological Institute (MNI) Structural atlas. This was a hypothesis-driven region-of-interest definition, based on the pain-selective effects in insula in a previous study using the same behavioral task (Perini et al. 2013). All other analyses within R221W carrier and control groups were performed at the whole brain level.

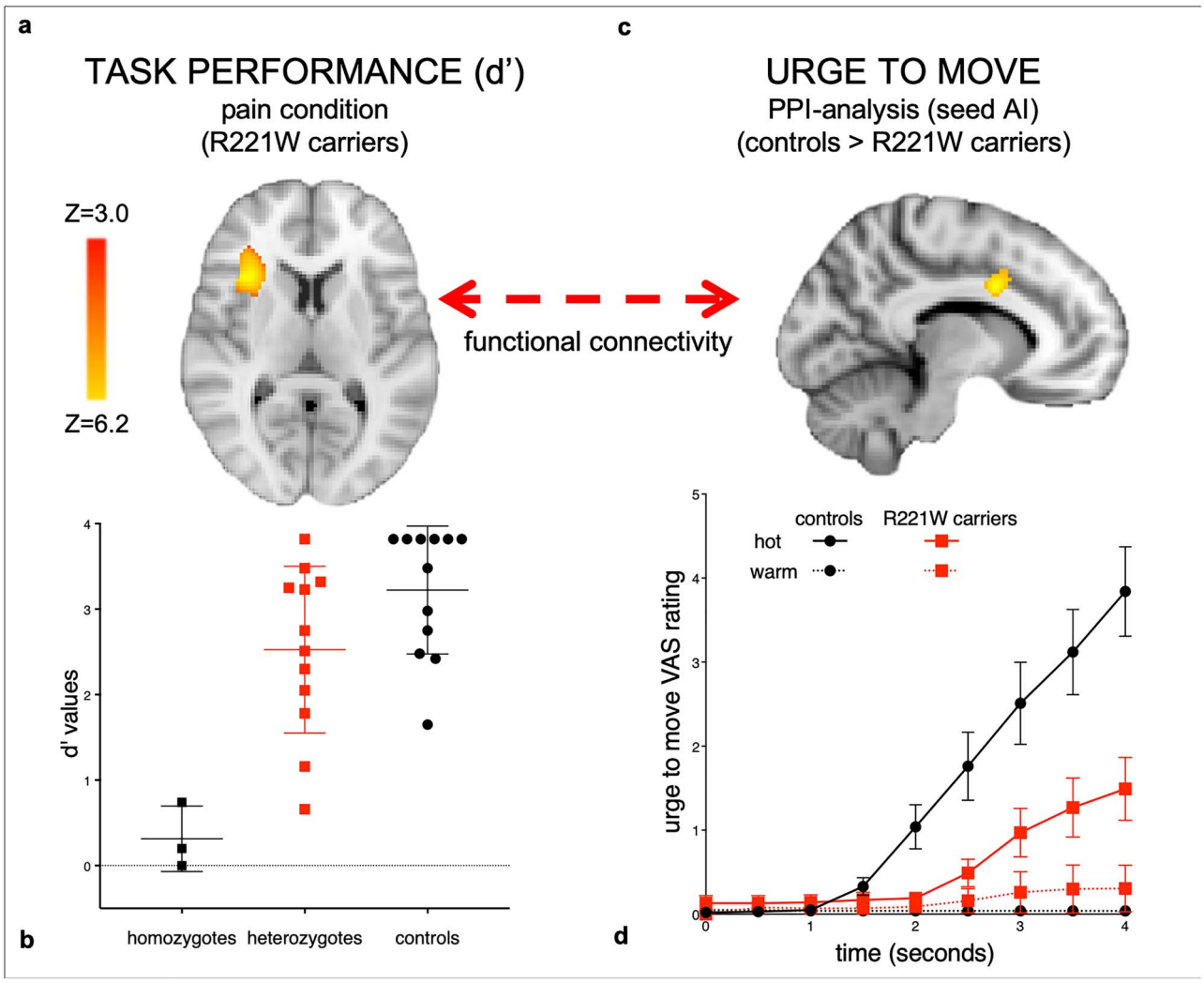

Figure 2. Cortical responses depending on signal-to-noise separation during painful stimulation and connectivity as a function of subjective escape urge. Heterozygous R221W carriers' broad variance on task performance (*b*) uncovers AI activation in signal-to-noise discrimination as a function of d′ (*a*). The closer the task-dependent signal-to-noise discrimination (as indexed by d′) to the healthy control range, the greater the activation in AI. To illustrate the full range of task performance variance in the R221W mutation phenotype, (*b*) also plots d′ data from a separate dataset of three homozygotes. The carriers' signal-sensitive AI activation cluster was used as a seed in a PPI analysis with "urge to move" slopes as covariates (*d*), revealing functional connectivity between AI and MCC during pain in controls (*c*), increasing as a function of the subjective urge to move away from the stimulus. No such interaction was seen in the carrier group, which reported a significantly lower and later urge to move during pain (*d*), VAS = visual analog scale rating of urge (adapted with permission from Testa et al. 2019). These results indicate that adaptive voluntary responses to pain rely on task-dependent signal-to-noise discrimination processes in AI, in conjunction with functional communication with MCC; impairment of this signal-to-action pathway may underlie the R221W carrier group's pain underreaction bias. Z statistic images were thresholded using clusters determined by $Z > 3.4$ and a (corrected) cluster significance threshold of $P = 0.05$, using the GRF theory (Worsley 2011).

The resulting cluster from this analysis, which covaried with R221W carriers' d′ scores, was used as a seed in a psychophysiological interaction (PPI) analysis (Friston et al. 1994; Friston et al. 1997; O'Reilly et al. 2012). A denoising procedure was first performed on all the runs using a probabilistic independent component analysis (ICA) (Beckmann and Smith 2004) implemented in MELODIC (Multivariate Exploratory Linear Optimized Decomposition into Independent Components) v3.14. The noise components were selected manually (Kelly Jr et al. 2010) and excluded from the following statistical analysis. The time course of the ROI for each run for each subject was then extracted and added to the analysis as physiological regressor, together with the four task regressors included in the original model (psychological regressors), four additional PPI regressors modeling the interaction between the ROI time course and the psychological regressors and d′ as a covariate. This PPI analysis probed the functional coupling of the seed cluster to other brain regions with respect to the ability to discern between task "signal" versus task "noise" stimuli (reflected by d′ scores). Similarly, a second PPI analysis probed the functional coupling of this cluster to the subjective motivation to escape a painful stimulus (urge to move). Individual mean slopes for "urge to move" ratings were calculated using linear regression and added as covariates in a model of the interaction between urge and the whole-brain BOLD time course, with the seed cluster defined by the d′ covariate analysis.

Functional Connectivity and Cortical Thickness Analyses

To further characterize functional network differences between groups, we also analyzed resting state connectivity, which reflects spontaneous functional connectivity across the whole brain in the absence of any task or stimulation. The resting state MRI data were preprocessed with the CONN toolbox version 15 (http://www.nitrc.org/projects/conn; Whitfield-Gabrieli and Nieto-Castanon 2020) implemented in SPM12 (Wellcome Trust Centre for Neuroimaging, London, United Kingdom) with the following steps: realignment, segmentation of anatomy images into gray and white matter and cerebrospinal fluid maps, normalization of anatomy and resting state images to an MNI template all resliced to 2-mm^3 voxel size, and smoothed with an 8-mmFWHM Gaussian kernel. We defined four task-derived ROIs for the ICA analysis, three atlas-based sensorimotor ROIs, and four parcellated anterior insula ROIs for the seed-based connectivity analysis in the following way: from the task-based analysis results, four ROIs were obtained by creating a 10-mm radius sphere around the peak activation voxel, for MCC (−8, 6, 32), right AI (32, 22, 6), left SI (−38, −30, 56), and left SII (−52, −22, 18). Three sensorimotor network ROIs were taken from the 90 fROI atlas from the FIND lab: right medial sensorimotor, left pre-/postcentral gyrus, and right pre-/postcentral gyrus (https://findlab.stanford.edu/functional_ROIs.html (Shirer et al. 2020). Four anterior insula ROIs were taken from a parcellation of the insula (Larsson et al. 2020): left and right dorsal anterior insula and left and right ventral anterior insula. Further analysis of a group ICA algorithm for the connectivity between the sensorimotor network and the task-derived ROIs was performed using the MATLAB-based GIFT toolbox version 3.0a (Medical Image Analysis Lab; http://mialab.mrn.org/software/gift). Default settings were used including subject-specific principal component analysis for data reduction, and 25 maximally spatially independent components were calculated with an infomax algorithm. Stability of ICA findings was ensured by rerunning ICA 100 times with the use of ICASSO; then the best stable run estimates were used to back-reconstruct components for each participant. The two components—a lateral and a posterior parietal component—that best matched the dorsal sensorimotor network from the 90 fROI atlas were selected for between-group analysis. The difference in connectivity pattern of the sensorimotor network between groups was initially thresholded at $P < 0.001$ with cluster extent > 20 voxels, and significance of connectivity differences in the four task-derived predefined ROIs was determined with the use of SPM12 small-volume corrections applied for each predefined ROI at $P < 0.0125$ Bonferroni-corrected ($\alpha = 0.05/11$) for the four tested ROIs and family-wise error (FWE) rate corrected for all voxels within each ROI.

Further exploratory investigations were done for whole-brain connectivity changes at the initial uncorrected threshold ($P < 0.001$ uncorrected, cluster extent > 20 voxels). Bilateral clusters of increased connectivity for carriers compared with controls at this uncorrected threshold were found in the lateral dorsal sensorimotor network with a cluster extent of 87 voxels (left; 52, −10, 14) and 122 voxels (right; −56, −2, 12). Analysis for seed-based correlations was performed using the ROI-to-ROI function in the CONN toolbox with default parameters. Preprocessed individual images were denoised by regressing out blood-oxygen level–dependent (BOLD) effects related to the white matter and CSF that are confounding to resting state, and the datasets were linearly detrended. Subject motion was filtered out from the data by regressing out the time series of the obtained realignment parameters with the use of ART scrubbing allowing for movement < 2 mm. Then, a band-pass filter of 0.008–0.09 Hz was applied. Bivariate correlations between ROIs were calculated on the weighted general linear model of the hemodynamic response function, and this data was entered into the second-level group analysis. ROI-to-ROI analysis of between-group differences was performed by investigating the connectivity between seeds and ROIs, both defined as our 11 predefined ROIs (4 task-derived, 3 sensorimotor, and 4 parcellated insula ROIs).

To explore the potential anatomical differences between groups, we performed a cortical thickness analysis. MRI data were preprocessed and analyzed using the freely available semiautomated pipeline FreeSurfer (https://surfer.nmr.mgh.harvard.edu/) (Fischl and Dale 2000). Briefly, preprocessing included intensity normalization, removal of nonbrain tissue, Talairach transformation, hemispheric separation, tissue segmentation, and tessellation of gray/white matter boundary. Cortical thickness was calculated as the distance between the white (white/gray matter border) and pial surface (gray matter/cerebrospinal fluid border) calculated for every point (vertex) for each hemisphere. Cortical maps were smoothed using a 10-mm FWHM Gaussian kernel. Cortical thickness comparison between controls and patients was conducted using a two-sample two-sided *t*-test, restricted to the insula cortex, defined by the Destrieux Atlas (Destrieux et al. 2010) as areas 47 (anterior insula), 17 and 18 (midposterior insula), and 48 (posterior insula), and tested separately for each hemisphere.

C Nerve Fiber Density (C-NFD)

We previously showed that, in a different sample of 19 R221W carriers, C-NFD correlated with self-reported evaluation of the painfulness of hypothetical pain situations (Perini et al. 2016), as measured by the Situated Pain Questionnaire (SPQ) (Clark and Yang 1983). In the previous study, carriers and healthy controls underwent corneal assessment with the Heidelberg Retina Tomograph (HRT III, Rostock cornea module) in vivo corneal confocal microscopy (Tavakoli and Malik 2011). Several scans of the entire depth of the cornea were recorded at ×800 magnification. The resulting images have a lateral resolution of 2 mm/pixel and a final image size of 400 × 400 pixels of the subbasal nerve plexus of the cornea from each subject. Quantification of C-NFD was based on six images per subject from the center of the cornea, which were examined in a masked and randomized fashion using purpose-written, proprietary software (CCMetrics; M. A. Dabbah, Imaging Science, University of Manchester). See Perini et al. (2016) for further details.

A subset of this sample (seven heterozygotes) participated in the present study. In addition, three homozygote carriers, presenting with a more severe pain phenotype (Minde et al. 2006), for whom C-NFD data had been collected had performed the present signal-to-noise task previously. Pooling the available data allowed a limited investigation of any relationship between behavioral (d′) and C-NFD measures in R221W carriers. For resting state data analysis, a subset of six carriers for whom both C-NFD resting state data had been collected, a regression analysis was performed with the C-NFD measures as a regressor added to the CONN ROI-to-ROI analysis described above. The correlation and regression analyses were corrected for age and gender, and significance was tested with two-tailed *t*-tests with a threshold of $P < 0.0045$ Bonferroni corrected ($\alpha = 0.05/11$) for the 11 tested

seed ROIs and false discovery rate (FDR) corrected for the 11 target ROIs.

Results

Behavioral Findings

Threshold testing revealed that human heterozygous R221W carriers showed a normal ability to discriminate noxious from innocuous thermal stimulation (Mann–Whitney; $U = 59$, $P = 0.4$ for innocuous, $U = 53$, $P = 0.2$ for painful). However, R221W carriers' task performance in terms of correct and incorrect responses was less accurate than controls' (χ^2 [2, 23] = 316.39, $P < 0.001$; incorrect presses when pain was signal [mean ± SD], carriers 0.23 ± 0.22, controls 0.10 ± 0.11, incorrect presses when pain was noise [mean ± SD], carriers 0.21 ± 0.15, controls 0.05 ± 0.07; Fig. 1*b*). Controls showed more skew toward higher task sensitivity in the distribution of d′ scores (controls −0.951, carriers −0.462). Controls also showed a larger, though trend-level, difference in task sensitivity than carriers between signal and noise distributions, as indexed by d′, (carriers 2.63 ± 0.99, controls 3.22 ± 0.75; $U = 43.0$, $P = 0.06$; Fig. 1*c*). Carriers had a larger bias to accept noise as signal, regardless of whether the stimulation was painful or nonpainful (criterion scores −1.69 for controls, −1.24 for carriers, $U = 26.5$, $P = 0.06$; Fig. 1*c*).

The relationship between C-NFD and d′ was not significant in the present subgroup of seven heterozygotes ($P > 0.9$). However, for the larger group of R221W carriers for which both C-NFD and d′ scores were available (including three homozygotes), C-NFD was positively correlated with d′ scores ($r = 0.75$, $P = 0.02$; Fig. 2*d*).

AI Discriminates Behavioral Relevance

In a previous study, the upper range of C-NFD measures in the heterozygous R221W carriers overlapped with the typical range in controls (Perini et al. 2016; Fig. 2*b*), indicating that a subset of the heterozygote population had a normal C-NFD phenotype. This is also implied by the decreased skew toward higher d′ scores observed here in the carrier group, which provided statistical traction for examining covariance of hemodynamic responses with these phenotypic measures. Covariance with higher scores might reveal functional activation in the typical phenotypic range, whereas lower scores would likely reflect mutation-linked functional perturbation. Regressing the R221W carriers' d′ scores onto whole-brain BOLD data revealed that signal in contralateral AI during painful stimulation versus baseline increased with performance accuracy in carriers compared with controls (Fig. 2*a*,*b*). In R221W carriers right AI (32, 22, 6) was positively correlated to d′ score values, indicating activation increases in this region with higher task sensitivity. The control group showed no significant activation, likely owing to a lower degree of variance on task performance. As expected, ceiling effects precluded this regression in the control group.

AI–Mid-ACC Functional Connectivity Increases with Motivational Escape Urgency

Urge to move slope values for painful heat stimulation were significantly different across groups ($U = 31$, $P = 0.01$). No difference was observed for warm temperature stimulation ($U = 63.5$, $P = 0.5$). Painful versus nonpainful stimulation in both groups elicited activation in regions robustly implicated in pain processing, including mid-ACC and AI (Table 1). However, in controls, the mid-ACC only responded to a stimulus if it was "signal" requiring a behavioral response, even for innocuous stimulation, replicating previous results (Perini et al. 2013; Fig. 3*a*, Tables 1 and 2). Controls but not R221W carriers showed significantly higher functional connectivity between AI and mid-ACC (−8, 6, 32), as reflected in the interaction between these time courses of these regions, together with additional premotor regions (Table 3), which covaried with motivational urge during pain.

Compensatory Sensorimotor Pathways in Carriers

A psychophysiological interaction (PPI) analysis (Friston et al. 1994; Friston et al. 1997; O'Reilly et al. 2012) was performed to investigate any interaction between the right AI cluster's time course and that of any other regions in the whole brain, as a function of urge to move ratings. With d′ as a PPI covariate, he AI seed cluster showed higher functional connectivity with right SII (56, −4, 4), in controls compared with R221W carriers. Consistent with this, controls had significantly thicker cortex in the left posterior insula (area 48, thickness [mean ± SD] controls 2.83 ± 0.20 mm, patients 2.67 ± 0.19 mm, $P = 0.026$; Fig. 4*b*).

In both groups, thermal painful compared with nonpainful stimulation activated brain regions classically involved in pain processing: the insular cortex bilaterally, somatosensory and premotor regions, cerebellum, and midbrain (Peyron et al. 2000). However, functional analyses revealed that R221W carriers showed significantly higher activity in primary motor and sensory cortices compared with controls (Table 1), most notably in a between-group, whole-brain comparison of responses for thermal painful versus nonpainful stimulation (the main effect of pain). Unlike the control group, R221W carriers showed no significant activation in medial prefrontal (including mid-ACC) and lateral premotor regions in a conjunction analysis between all "signal" conditions regardless of pain. Similar to our previous investigation, the controls showed motor-specific activations in MCC together with premotor and sensory areas ([−8, 6, 40]; Table 2, Fig. 3*a*). Carriers showed no significant activation in these medial and lateral premotor regions, with activation limited to the left primary somatosensory and motor cortices (−38, −30, 56) and the left SII ([−52, −22, 18]; Fig. 3*b*, Table 2). Together with the main effect of pain results, the conjunction analysis may indicate compensatory processing related to direct motor output in the task.

R221W carriers showed greater resting state connectivity than controls in left SI within the posterior parietal dorsal sensorimotor network (peak level $P = 0.006$ family-wise error [FWE]-corrected within the SI ROI). Increased bilateral operculum connectivity for R221W carriers compared with controls in the lateral dorsal sensorimotor network was observed in a whole-brain exploratory analysis ($P < 0.001$, uncorrected).

In the subset of six R221W carriers for whom measures were available, R221W carriers with lower C-NFD showed higher functional connectivity between left dorsal anterior insula and right sensorimotor cortex ($P = 0.003$ FDR-corrected).

Discussion

These findings provide evidence in support of the idea that cortical processing of acute pain is shaped not just by the nociceptive signal but by the relevance of the stimulus to current behavior. This is consistent with research demonstrating that cortical pain processing is influenced by factors such as voluntary attentional focus (Kulkarni et al. 2005), expectation (Ploghaus et al. 1999; Wiech et al. 2010), social factors (Krahe et al. 2013), and other

Table 1 Activations during "painful stimulation" (pain > nonpain)

Analysis	Peak coordinates (*x*, *y*, *z*)	Cluster size
Controls		
Painful stimulation		
		Cluster #1
Superior frontal gyrus (pre-SMA)	5.05 (4, 22, 58)	1888
Superior frontal gyrus (SMA)	4.88 (6, 8, 58)	
Superior frontal gyrus	4.72 (4, 32, 54)	
Anterior cingulate cortex	4.67 (0, 30, 30)	
Midcingulate cortex	4.05 (6, 22, 40)	
Superior frontal gyrus (pre-SMA)	3.72 (−10, 14, 64)	
		Cluster #2
Anterior insula	5.66 (−36, 16, −6)	1106
Anterior insula	5.23 (−36, 24, −6)	
Anterior insula	4.82 (−32, 24, 4)	
Anterior superior temporal gyrus	4.29 (−54, 12, −8)	
Inferior frontal gyrus (pars opercularis)	3.45 (−60, 4, 0)	
Frontal operculum	3.26 (−52, 0, 2)	
		Cluster #3
Midbrain	5.31 (2,-20,-18)	877
Midbrain	4.27 (10, −24, −10)	
Midbrain	3.9 (−6, −30, −14)	
Midbrain	3.71 (10, −16, −16)	
Midbrain	3.67 (−6, −8,-8)	
Carriers		
Painful stimulation		
		Cluster #1
Superior frontal gyrus (SMA)	7.6 (2, 10, 52)	18 155
Anterior insula	7.05 (−38, 14, −2)	
Mid-insula	6.81 (34, 6, 16)	
Anterior superior temporal gyrus	6.73 (−54, 12, −2)	
Frontal operculum	6.66 (50, 8, 2)	
Anterior insula	6.63 (34, 20, 6)	
Carriers > controls		
Painful stimulation		
		Cluster #1
Postcentral gyrus (BA 3b)	6.49 (56,-6, 22)	1230
Inferior frontal gyrus (pars opercularis)	4.91 (62, 8, 4)	
Precentral gyrus	4.1 (46, −16, 64)	
Postcentral gyrus (BA 4)	3.92 (42, −14, 48)	
Precentral gyrus (BA 6)	3.8 (38, −24, 70)	
Precentral gyrus (BA 6)	3.63 (52, −8, 44)	

Note: All reported clusters $Z > 3$, $P = 0.01$ whole-brain cluster corrected (MNI coordinates). SMA, supplementary motor area; BA, Brodmann area

Table 2 Conjunction analysis

Analysis	Peak coordinates (*x*, *y*, *z*)	Cluster size
Conjunction pain-press ∩ non–pain-press (controls)		
		Cluster #1
Precentral gyrus (MI)	8.93 (−46, −20, 62)	6320
Supplementary motor cortex	(−4, −8, 56)	
Midcingulate cortex	(−8, 6, 40)	
		Cluster #2
Cerebellum lobule V	8.47 (18, −52, −22)	3253
		Cluster #3
Brainstem	4.36 (−10, −26, −8)	1409
Conjunction pain-press ∩ non–pain-press (carriers)		
		Cluster #1
Pre-/postcentral gyrus (SI/MI)	7.76 (−38, −30, 56)	2625

Activations showing shared motor activity to painful and nonpainful stimulation. All reported clusters $Z > 3$, $P = 0.01$ whole-brain cluster corrected (MNI coordinates). MI, primary motor cortex; SI, primary somatosensory cortex

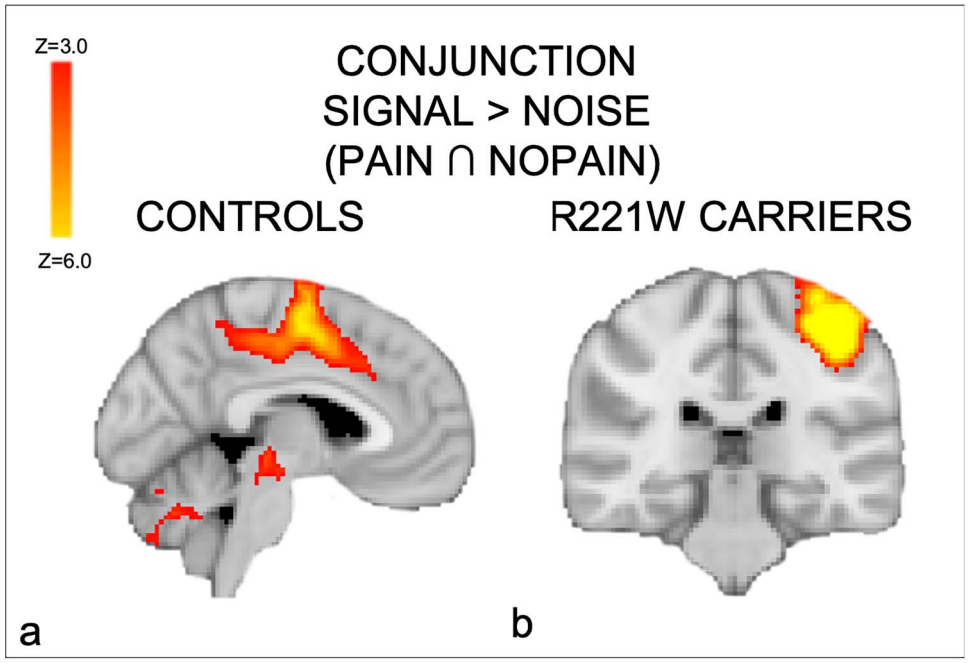

Figure 3. Conjunction of "signal" conditions in which the task required an action (button press), regardless of whether the stimulus was painful or nonpainful. (*a*) Activation in the mid-ACC, premotor, and subcortical regions in controls. (*b*) R221W carriers showed activations in MI as well as in SII, contralateral to the response hand. These findings suggest a compensatory role for these regions in context-dependent voluntary responses during pain.

Table 3 PPI analysis results

Analysis	Peak coordinates (*x*, *y*, *z*)	Cluster size
PPI (controls > carriers) covariate: urge to move		
Painful stimulation		
		Cluster #1
Midcingulate cortex	4.58 (−8, 6, 32)	416
Supplementary motor area	3.90 (−4, 8, 50)	
Supplementary motor area	3.64 (−4, −2, 50)	

Activations showing high temporal synchrony with the right anterior insula (AI) during "painful stimulation." All reported clusters $Z > 3$, $P = 0.01$ whole-brain cluster corrected (MNI coordinates)

contextual factors (Woo et al. 2017). With respect to the effects of the R221W mutation on the nervous system organization of heterozygous carriers, these findings further suggest that any presentation of pain indifference (Minde et al. 2004) may be attributed to an individually variable impairment in translating nociceptive afferent signaling into situation-appropriate behavioral responses, rather than to an impairment in the ability to perceive and report nociceptive stimulation.

Despite reporting normal pain thresholds, R221W carriers' task performance was worse than controls', and their subjective motivational urge to escape the noxious stimulation was lower. Carriers also showed a lower signal sensitivity on the task, as indexed by d′ scores, regardless of whether the "signal" stimulus was painful. Carriers' pattern of errors also displayed a bias to respond to stimuli which the task required them to disregard. This suggests that a certain degree of uncertainty, perhaps in the form of a reduced signal-to-noise ratio, may have interfered with task sensitivity for both painful and nonpainful stimuli. d′ as an index of task performance also correlated with peripheral C-NFD in a subset of seven R221W carriers (including three homozygotes) for which these data were available. The upper range of both task performance and C-NFD measures in the carriers overlapped with the typical range (Fig. 2*b*). Carriers with higher task performance showed increased activation in the contralateral AI cortex. This region showed higher functional connectivity with mid-ACC as a function of increased motivational escape urge during pain, but in controls only. As a group, carriers showed lower BOLD responses in AI and mid-ACC, as well as thinner cortex in the posterior insula. However, they also displayed a bias toward greater engagement of sensorimotor cortices during pain, implying a compensatory role for these regions in pain–action integration.

Sensitivity to Task Variables in Mid-ACC and AI

AI and midanterior cingulate cortex are the regions most likely to be activated in fMRI studies in both healthy and patient groups (Knudsen et al. 2018), but their joint functional roles have remained unclear. Here, the engagement of the mid-ACC in controls showed preferential responses to "signal" stimuli—those for which an overt behavioral response was required—even for innocuous stimulation. This replicates previous normative results, which indicate that mid-ACC responses to pain depend on the modulation of behavioral response execution. Perini et al. (2013) demonstrated that regions of ACC and midcingulate cortex (MCC) did not respond to pain unless an overt motor response was required by the task. Importantly, this region of the MCC contains premotor fields, among them the putative caudal cingulate motor zone (CMZ). The premotor properties of CMZ, alongside a correlation of CMZ BOLD changes with reaction times for "signal" stimuli regardless of whether they were painful (Perini et al. 2013), underscore the idea that

the role of this region in pain processing lies in the selection, preparation, and execution of voluntary behavioral responses (in this case, to press or not to press the button). Crucially, although the midcingulate cortex exhibits pain-specific, yet generalizable, activation patterns compared with negative emotion and cognitive control (Kragel et al. 2018), controlling for motor processing in this study indicated that its predominantly premotor role was *not* specific for pain (e.g., Mouraux et al. 2011; Wager et al. 2016; see also Salomons et al. 2020).

The carrier's neural responses shed light on the functional role of AI during acute pain. As in the previous normative study (Perini et al. 2013), AI was activated for painful versus nonpainful stimulation in a main effect contrast. The interpretation of this main effect of pain in healthy controls was limited by the fact that this group's task performance was at ceiling. Here, however, the decreased skew toward ceiling within the R221W carrier group's d′ scores allowed us to probe the underlying functional processing. Specifically, it enabled the examination of whether the main effect of pain in the AI reflected a simple selectivity for sensory nociceptive information (pain vs. nonpain) or an engagement by nociceptive stimulation which also involved a critical sensitivity to task. The latter alternative would indicate that a difference in pain–action integration underlies differences in task performance between groups. It would also imply that the difference would lie at a relatively early stage in a cortical processing hierarchy of the incoming nociceptive signal.

Examining activation in the R221W carriers as a function of performance (d′) revealed that AI did exhibit task sensitivity, discriminating task-relevant from task-irrelevant stimulus features during pain. In effect, this region lifted "signal" from "noise" against a backdrop of sensory stimulation. The lower an individual's task sensitivity, the less the AI was engaged. AI's ability to filter behaviorally relevant and irrelevant sensory stimulation here is consistent with its proposed role in the processing of task-relevant, salient stimuli (Seeley et al. 2007; Mouraux et al. 2011; Uddin 2015; Wager et al. 2016; Salomons et al. 2020), where "salience" may reflect underlying signal-to-noise processing. It is also consistent with human neuroimaging evidence suggesting that AI activity predicts whether a subject will classify a stimulus as painful, biasing "perceptual decisions" about pain even before the stimulus occurs (Wiech et al. 2010, 2014), and that context-dependent functional connectivity increases between AI and different cortical networks during pain (Ploner et al. 2011). On a network level, the AI is a key hub implicated in task-set maintenance (Dosenbach et al. 2008), consistent with a supervenient influence of behavioral goals upon stimulus processing.

Controls' cortical thickness was greater in the posterior insula. The posterior insula is likely a primary target of thalamocortical pain pathways (Craig and Zhang 2006; Dum et al. 2009). Processing in the insular cortex has also been linked to pain evaluation, as well as the subjective experience of pain (Bancaud et al. 1976; Mazzola et al. 2012; Frot et al. 2014; Segerdahl et al. 2015). The PI is likely a main cortical hub for integration of nociceptive information into subjective (Craig 2003) and autonomic (Critchley et al. 2004) efferent terms.

Following the fMRI session, participants were asked to continuously rate their urge to withdraw the stimulated hand away from the thermode during stimulation, in trials structured exactly like those in the main experiment. This task was designed to capture any subjective motivational impetus to action instigated by painful or nonpainful thermal stimulation. Although these measurements were performed outside the scanner and therefore cannot reflect direct relationships with hemodynamic changes, they were used as indices of interindividual variation in motivational urges and modeled as covariants in the BOLD data. Using the task-sensitive AI cluster as a seed region, a PPI functional connectivity analysis using "urge to move" as an interaction term showed that AI activation in controls synchronizes with mid-ACC activation as a function of individuals' subjective withdrawal urge reports during painful stimulation (Fig. 2*c*). This was not the case in carriers, who reported significantly lower motivational urges (Fig. 2*d*). This may reflect a joint role for AI and mid-ACC in producing motivated, subjectively "hot" representations characteristic of pain experience, with AI signaling high behavioral relevance of a stimulus, and mid-ACC selecting and prioritizing voluntary actions on this basis (Morrison et al. 2013).

R221W Carriers Engage Sensorimotor Network Adequate for Behavior but not Motivation

We further interrogated this relationship by exploring how central the AI–mid-ACC network's observed contribution to motivated response selection in controls may be for producing appropriate pain behavior on the task in the R221W carrier group. In contrast to the prominent insular involvement in controls, R221W carriers showed greater engagement of a network involving lateral and primary sensorimotor cortices for the main effect of pain, as well as for producing voluntary behavioral responses regardless of pain. The lower an individual carriers' C-NFD, the greater the connectivity within this sensorimotor network, particularly between left dorsal AI and right primary sensory and motor cortices, though the statistical significance of this effect may be inflated by the small group size. If reliable, this relationship may indicate a greater compensatory involvement in individuals with lower reported motivational impetus to take action to escape pain. Taken together, however, these findings suggest that carriers may rely disproportionately on processing in sensorimotor networks during the integration of sensory and other behaviorally relevant information. This is consistent with a transgenic mouse model of the mutation which indicated a selective deficit in pain-related fear conditioning alongside reduced neuronal activity in motor, but not sensory, cortex (Testa et al. 2019).

The carrier group's relatively subtle behavioral deficits on the task suggest an overall adequacy of this network for producing behavior in the presence of a sensory stimulus. However, the significant costs in performance accuracy, alongside the markedly higher latency and reduction in subjective urgency for pain, imply that this alternate network nonetheless integrates stimulus- and task-related information with behavior "less efficiently." A possibility to be addressed by future research is that R221W carriers may evaluate pain on a linear intensity scale, supported by sensorimotor networks, rather than in terms of a motivation- or behavior-centered threshold, supported by the AI–mid-ACC axis. In contrast, typical-range processing in the insula–cingulate network probably achieves a more seamless and rapid integration of stimulus processing and behavioral relevance, stamped with motivational impetus. While not specific for pain, this network is likely optimally suited for efficient, high signal-to-noise, high-gain processing of behaviorally relevant signals, thus occupying a central functional role in adaptive, flexible behavioral changes to noxious events (Shackman et al. 2011; Morrison et al. 2013).

Conclusions

In heterozygous R221W carriers, the relationship between pain and action is disrupted at the level of cortical integration of the stimulus, though their pain thresholds do not differ from controls'. A possible explanation is that reduced C-afferent input to central pathways may result in greater signal uncertainty in the brain during integration of stimulus- and task-related features. Such diminished signal-to-noise differentiation in the AI, however subtle, may introduce bias or alter the weighting of the signal, perhaps predictively (Roy et al. 2014; Eldar et al. 2016), thus shifting a decision criterion and increasing the likelihood of classifying noise as signal in the task. Rather than affecting specific neural populations or brain regions, though, we speculate that these effects likely propagate through networks receiving predominant projections from C-afferent pathways, particularly within an insula–cingulate network, thus influencing wider network-level signaling. R221W carrier brains may compensate via an increased contribution from dorsolateral sensorimotor networks during pain–action integration. Though adequate for task performance, this contribution may be inefficient for the production of motivated behavior, in contrast with the contribution of motivational–affective processing in the insula–cingulate network observed in controls and high-performing carriers.

Funding

Swedish Research Council (grant VR 2010-2120 to I.M.).

Notes

The authors thank the Umeå Center for Functional Brain Imaging (UFBI) (particularly Lars Nyberg and Johan Ericsson), Karin Göthner, Tomas Karlsson, Monica Holmberg, Ignacio Serrano-Pedraza, Loki, and the carrier volunteers. They thank also Ellen Lumpkin and Patric Bach for their valuable comments on an earlier draft.

Competing Interests

The authors declare no competing interests.

References

Atlas LY, Bolger N, Lindquist MA, Wager TD. 2010. Brain mediators of predictive cue effects on perceived pain. *J Neurosci*. 30(39):12964–12977. doi: 10.1523/JNEUROSCI.0057-10.2010.

Bancaud J, Talairach J, Geier S, Bonis A, Trottier S, Manrique M. 1976. Behavioral manifestations induced by electric stimulation of the anterior cingulate gyrus in man—Abstract. *Rev Neurol (Paris)*. 132(10):705–724.

Beckmann CF, Jenkinson M, Smith SM. 2003. General multilevel linear modeling for group analysis in FMRI. *NeuroImage*. 20(2):1052–1063. doi: 10.1016/s1053-8119(03)00435-x.

Beckmann CF, Smith SM. 2004. Probabilistic independent component analysis for functional magnetic resonance imaging. *IEEE Trans Med Imaging*. 23:137–152.

Clark WC, Yang JC. 1983. Applications of sensory detection theory to problems in laboratory and clinical pain. In: Melzack R, editor. *Pain measurement and assessment*. New York: Raven Press, pp. 15–25.

Craig AD. 2003. A new view of pain as a homeostatic emotion. *Trends Neurosci*. 26(6):303–307.

Craig AD, Zhang ET. 2006. Retrograde analyses of spinothalamic projections in the macaque monkey: input to posterolateral thalamus. *J Comp Neurol*. 499(6):953–964. doi: 10.1002/cne.21155.

Critchley HD, Wiens S, Rotshtein P, Ohman A, Dolan RJ. 2004. Neural systems supporting interoceptive awareness. *Nat Neurosci*. 7(2):189–195. doi: 10.1038/nn1176.

Destrieux C, Fischl B, Dale A, Halgren E. 2010. Automatic parcellation of human cortical gyri and sulci using standard anatomical nomenclature. *Neuroimage*. 53:1–15. doi: 10.1016/j.neuroimage.2010.06.010.

Dosenbach NU, Fair DA, Cohen AL, Schlaggar BL, Petersen SE. 2008. A dual-networks architecture of top-down control. *Trends Cogn Sci*. 12(3):99–105. doi: 10.1016/j.tics.2008.01.001.

Dum RP, Levinthal DJ, Strick PL. 2009. The spinothalamic system targets motor and sensory areas in the cerebral cortex of monkeys. *J Neurosci*. 29(45):14223–14235. doi: 10.1523/JNEUROSCI.3398-09.2009.

Eldar E, Hauser TU, Dayan P, Dolan RJ. 2016. Striatal structure and function predict individual biases in learning to avoid pain. *Proc Natl Acad Sci USA*. 113(17):4812–4817. doi: 10.1073/pnas.1519829113.

Fischl B, Dale AM. 2000. Measuring the thickness of the human cerebral cortex from magnetic resonance images. *Proc Natl Acad Sci USA*. 97:11050–5.

Friston KJ, Buechel C, Fink GR, Morris J, Rolls E, Dolan RJ. 1997. Psychophysiological and modulatory interactions in neuroimaging. *NeuroImage*. 6(3):218–229. doi: 10.1006/nimg.1997.0291.

Friston KJ, Holmes AP, Worsley KJ, Poline JP, Frith CD, Frackowiak RSJ. 1994. Statistical parametric maps in functional imaging: a general linear approach. *Hum Brain Mapp*. 2(4):189–210. doi: 10.1002/hbm.460020402.

Frot M, Faillenot I, Mauguiere F. 2014. Processing of nociceptive input from posterior to anterior insula in humans. *Hum Brain Mapp*. 35(11):5486–5499. doi: 10.1002/hbm.22565.

Green DM, Swets JA. 1966. *Signal detection theory and psychophysics*. New York, USA: John Wiley and Sons.

Grush R. 2004. The emulation theory of representation: Motor control, imagery, and perception. *Behavioral and Brain Sciences*. 27:377–396.

Hall TS. 1972. *Treatise of man*. Cambridge: Harvard University Press.

Jenkinson M, Bannister P, Brady M, Smith S. 2002. Improved optimization for the robust and accurate linear registration and motion correction of brain images. *NeuroImage*. 17(2):825–841.

Kelly RE Jr, Alexopoulos GS, Wang Z, Gunning FM, Murphy CF, Morimoto SS, *et al*. 2010. Visual inspection of independent components: defining a procedure for artifact removal from fMRI data. *J Neurosci Method*. 189(2):233–245. doi: 10.1016/j.jneumeth.2010.03.028.

Knudsen L, Petersen GL, Norskov KN, Vase L, Finnerup N, Jensen TS, Svensson P. 2018. Review of neuroimaging studies related to pain modulation. *Scand J Pain*. 2(3):108–120. doi: 10.1016/j.sjpain.2011.05.005.

Kragel PA, Kano M, Van Oudenhove L, Ly HG, Dupont P, Rubio A, *et al*. 2018. Generalizable representations of pain, cognitive control, and negative emotion in medial frontal cortex. *Nat Neurosci*. 21(2):283–289. doi: 10.1038/s41593-017-0051-7.

Krahe C, Springer A, Weinman JA, Fotopoulou A. 2013. The social modulation of pain: others as predictive signals of salience—a systematic review. *Front Hum Neurosci*. 7:386. doi: 10.3389/fnhum.2013.00386.

Kulkarni B, Bentley DE, Elliott R, Youell P, Watson A, Derbyshire SW, *et al*. 2005. Attention to pain localization and unpleasantness discriminates the functions of the medial and lateral pain systems. *Eur J Neurosci*. 21(11):3133–3142. doi: 10.1111/j.1460-9568.2005.04098.x.

Larsson E, Kuma R, Norberg A, Minde J, Holmberg M. 2009. Nerve growth factor R221W responsible for insensitivity to pain is defectively processed and accumulates as proNGF. *Neurobiol Dis*. 33(2):221–228. doi: 10.1016/j.nbd.2008.10.012.

Larsson MB, Tillisch K, Craig AD, Engström M, Labus J, Naliboff B, Lundberg P, *et al*. 2020. Brain responses to visceral stimuli reflect visceral sensitivity thresholds in patients with irritable bowel syndrome. 1528-0012 (Electronic).

Lopez-Sola M, Geuter S, Koban L, Coan JA, Wager TD. 2019. Brain mechanisms of social touch-induced analgesia in females. *Pain*. 160(9):2072–2085. doi: 10.1097/j.pain.0000000000001599.

Mazzola L, Isnard J, Peyron R, Mauguiere F. 2012. Stimulation of the human cortex and the experience of pain: Wilder Penfield's observations revisited. *Brain J Neurol*. 135(Pt 2):631–640. doi: 10.1093/brain/awr265.

Minde J, Svensson O, Holmberg M, Solders G, Toolanen G. 2006. Orthopedic aspects of familial insensitivity to pain due to a novel nerve growth factor beta mutation. *Acta Orthop*. 77(2):198–202. doi: 10.1080/17453670610045911.

Minde J, Toolanen G, Andersson T, Nennesmo I, Remahl IN, Svensson O, Solders G. 2004. Familial insensitivity to pain (HSAN V) and a mutation in the NGFB gene. A neurophysiological and pathological study. *Muscle Nerve*. 30(6):752–760. doi: 10.1002/mus.20172.

Morrison I, Perini I, Dunham J. 2013. Facets and mechanisms of adaptive pain behavior: predictive regulation and action. *Front Hum Neurosci*. 7:755. doi: 10.3389/fnhum.2013.00755.

Mouraux A, Diukova A, Lee MC, Wise RG, Iannetti GD. 2011. A multisensory investigation of the functional significance of the "pain matrix". *NeuroImage*. 54(3):2237–2249. doi: 10.1016/j.neuroimage.2010.09.084.

Nöe A. 2004. *Action in Perception*. Cambridge: MIT Press.

O'Reilly JX, Woolrich MW, Behrens TE, Smith SM, Johansen-Berg H. 2012. Tools of the trade: psychophysiological interactions and functional connectivity. *Soc Cogn Affect Neurosci*. 7(5):604–609. doi: 10.1093/scan/nss055.

Perini I, Bergstrand S, Morrison I. 2013. Where pain meets action in the human brain. *J Neurosci*. 33(40):15930–15939. doi: 10.1523/JNEUROSCI.3135-12.2013.

Perini I, Tavakoli M, Marshall A, Minde J, Morrison I. 2016. Rare human nerve growth factor-beta mutation reveals relationship between C-afferent density and acute pain evaluation. *J Neurophysiol*. 116(2):425–430. doi: 10.1152/jn.00667.2015.

Peyron R, Laurent B, Garcia-Larrea L. 2000. Functional imaging of brain responses to pain. A review and meta-analysis (2000). *Neurophysiol Clin*. 30(5):263–288.

Ploghaus A, Tracey I, Gati JS, Clare S, Menon RS, Matthews PM, Rawlins JN. 1999. Dissociating pain from its anticipation in the human brain. *Science*. 284(5422):1979–1981. doi: 10.1126/science.284.5422.1979.

Ploner M, Lee MC, Wiech K, Bingel U, Tracey I. 2011. Flexible cerebral connectivity patterns subserve contextual modulations of pain. *Cereb Cortex*. 21(3):719–726. doi: 10.1093/cercor/bhq146.

Prinz W. 1997. Perception and action planning. *Eur J Cogn Psychol*. 9:129–154.

Roy M, Shohamy D, Daw N, Jepma M, Wimmer GE, Wager TD. 2014. Representation of aversive prediction errors in the human periaqueductal gray. *Nat Neurosci*. 17(11):1607–1612. doi: 10.1038/nn.3832.

Salomons TV, Iannetti GD, Liang M, Wood JN. 2020 The "pain matrix" in pain-free individuals. 2168-6157 (Electronic).

Seeley WW, Menon V, Schatzberg AF, Keller J, Glover GH, Kenna H, *et al*. 2007. Dissociable intrinsic connectivity networks for salience processing and executive control. *J Neurosci*. 27(9):2349–2356. doi: 10.1523/JNEUROSCI.5587-06.2007.

Segerdahl AR, Mezue M, Okell TW, Farrar JT, Tracey I. 2015. The dorsal posterior insula subserves a fundamental role in human pain. *Nat Neurosci*. 18(4):499–500. doi: 10.1038/nn.3969.

Seminowicz DA, Mikulis DJ, Davis KD. 2004. Cognitive modulation of pain-related brain responses depends on behavioral strategy. *Pain*. 112(1–2):48–58. doi: 10.1016/j.pain.2004.07.027.

Shackman AJ, Salomons TV, Slagter HA, Fox AS, Winter JJ, Davidson RJ. 2011. The integration of negative affect, pain and cognitive control in the cingulate cortex. *Nat Rev Neurosci*. 12(3):154–167. doi: 10.1038/nrn2994.

Shirer WR, Ryali S, Rykhlevskaia E, Menon V, Greicius MD. 2020 Decoding subject-driven cognitive states with whole-brain connectivity patterns. 1460-2199 (Electronic).

Sinke C, Forkmann K, Schmidt K, Wiech K, Bingel U. 2016. Expectations impact short-term memory through changes in connectivity between attention- and task-related brain regions. *Cortex*. 78:1–14. doi: 10.1016/j.cortex.2016.02.008.

Smith SM. 2002. Fast robust automated brain extraction. *Hum Brain Mapp*. 17(3):143–155. doi: 10.1002/hbm.10062.

Sullivan MJ. 2008. Toward a biopsychomotor conceptualization of pain: implications for research and intervention. *Clin J Pain*. 24(4):281–290. doi: 10.1097/AJP.0b013e318164bb15.

Sung K, Ferrari LF, Yang W, Chung C, Zhao X, Gu Y, *et al*. 2018. Swedish nerve growth factor mutation (NGF(R100W)) defines a role for TrkA and p75(NTR) in nociception. *J Neurosci*. 38(14):3394–3413. doi: 10.1523/JNEUROSCI.1686-17.2018.

Tavakoli M, Malik RA. 2011. Corneal confocal microscopy: a novel non-invasive technique to quantify small fibre pathology in peripheral neuropathies. *J Vis Exp*. 47:pii: 2194.

Taylor VA, Chang L, Rainville P, Roy M. 2017. Learned expectations and uncertainty facilitate pain during classical conditioning. *Pain*. 158(8):1528–1537. doi: 10.1097/j.pain.0000000000000948.

Testa G, Mainardi M, Morelli C, Olimpico F, Pancrazi L, Petrella C, *et al*. 2019. The NGF(R100W) mutation specifically impairs nociception without affecting cognitive performance in a mouse model of hereditary sensory and autonomic neuropathy type V. *J Neurosci*. 39(49):9702–9715. doi: 10.1523/JNEUROSCI.0688-19.2019.

Uddin LQ. 2015. Salience processing and insular cortical function and dysfunction. *Nat Rev Neurosci*. 16(1):55–61. doi: 10.1038/nrn3857.

Wager TD, Atlas LY, Botvinick MM, Chang LJ, Coghill RC, Davis KD, *et al*. 2016. Pain in the ACC? *Proc Natl Acad Sci USA*. 113(18):E2474–E2475. doi: 10.1073/pnas.1600282113.

Whitfield-Gabrieli S, Nieto-Castanon A. 2020 Conn: a functional connectivity toolbox for correlated and anticorrelated brain networks. 2158-0022 (Electronic).

Wickens TD. 2001. *Elementary signal detection theory*. Oxford, UK: Oxford University Press.

Wiech K, Lin CS, Brodersen KH, Bingel U, Ploner M, Tracey I. 2010. Anterior insula integrates information about salience into perceptual decisions about pain. *J Neurosci*. 30(48):16324–16331. doi: 10.1523/jneurosci.2087-10.2010.

Wiech K, Tracey I. 2013. Pain, decisions, and actions: a motivational perspective. *Frontiers in neuroscience*. 7:46. doi: 10.3389/fnins.2013.00046.

Wiech K, Vandekerckhove J, Zaman J, Tuerlinckx F, Vlaeyen JW, Tracey I. 2014. Influence of prior information on pain involves biased perceptual decision-making. *Curr Biol*. 24(15):R679–R681. doi: 10.1016/j.cub.2014.06.022.

Woo CW, Schmidt L, Krishnan A, Jepma M, Roy M, Lindquist MA, *et al*. 2017. Quantifying cerebral contributions to pain beyond nociception. *Nat Commun*. 8:14211. doi: 10.1038/ncomms14211.

Woolrich M. 2008. Robust group analysis using outlier inference. *NeuroImage*. 41(2):286–301. doi: 10.1016/j.neuroimage.2008.02.042.

Woolrich MW, Behrens TE, Beckmann CF, Jenkinson M, Smith SM. 2004. Multilevel linear modelling for FMRI group analysis using Bayesian inference. *NeuroImage*. 21(4):1732–1747. doi: 10.1016/j.neuroimage.2003.12.023.

Worsley KJ. 2011. Statistical analysis of activation images. In: Jezzard P, Matthews PM, Smith SM, editors. *Functional MRI: an introduction to methods*. Oxford Scholarship Online. doi: 10.1093/acprof:oso/9780192630711.001.0001.

Zaman J, Wiech K, Claes N, Van Oudenhove L, Van Diest I, Vlaeyen JWS. 2018. The influence of pain-related expectations on intensity perception of nonpainful somatosensory stimuli. *Psychosom Med*. 80(9):836–844. doi: 10.1097/PSY.0000000000000586.